In Vivo Study of HIV-1 Tat Arginine-rich Motif Unveils Its Transport Properties

Francesco Cardarelli[1,2], Michela Serresi[1], Ranieri Bizzarri[1,2], Mauro Giacca[2,*] and Fabio Beltram[1,2]

[1]*Scuola Normale Superiore and Italian Institute of Technology, Pisa, Italy;* [2]*Scuola Normale Superiore and NEST INFM-CNR, Pisa, Italy*

Tat-derived peptides have attracted much interest as molecular carriers for intracellular delivery as they incorporate specific attributes required for efficient cargo delivery to sub-cellular domains. Little is known, however, about intracellular trafficking and interactions of Tat peptide–tagged cargoes, although some *in vitro* studies have suggested the relevance of active processes in Tat peptide–driven nuclear translocation. These issues are addressed by comparing Tat peptide–induced transport properties with well-established passive diffusion and active import benchmarks in living cells. Specifically, we examine several constructs of increasing molecular weight (MW) both below and above the threshold for passive diffusion through the nuclear pore. The resulting sub-cellular localization is analyzed by confocal imaging, and construct intracellular dynamics is investigated by fluorescence recovery after photobleaching (FRAP) real-time imaging. Our experiments yield the characteristic transport parameters of Tat peptide intra-cytoplasm dynamics and nucleus/cytoplasm shuttling. These results allow us to elucidate the mechanism of Tat peptide–driven nuclear permeation, demonstrating that it crosses the nuclear envelope (NE) by passive diffusion. Finally, we discuss the limitations of this route in terms of acceptable cargo size.

Received 9 January 2007; accepted 14 March 2007; published online 1 May 2007. doi:10.1038/sj.mt.6300172

INTRODUCTION

The Tat protein of human immunodeficiency virus type 1 is a powerful transcriptional activator of viral gene expression and enhances the rate of human immunodeficiency virus type 1 long terminal repeat–specific transcription.[1,2] In addition to this critical role as a transcription factor, a growing body of evidence suggests that Tat plays a role as an extracellular protein. In fact, Tat is readily taken up by cells through interactions with heparin sulfate proteoglycans displayed on the cell membrane and then develops a number of peculiar interactions with specific cell proteins.[3,4]

Cell penetration depends upon the integrity of the basic region of the protein (YG**RKKRR**Q**RRR**, basic residues in bold). This arginine-rich sequence also corresponds to the presumed nuclear localization signal (NLS) and the trans-activation responsive region binding domain of the protein.[5] The growing interest in the cell-penetrating properties of this peptide is due to its ability to drive the internalization of a large variety of cargoes chemically coupled or fused to it in mammalian and human cell types.[6] Data indicate that the Tat peptide can determine cellular uptake of non-permeant molecules and lead to the expected biological response, consistent with the internalization of intact peptide-cargo fusions.[7,8] Despite the variety of biotechnological applications of the Tat peptide as a delivery vector, little is known about the intracellular behavior and fate of Tat peptide–based chimeras. As mentioned, the Tat peptide is a putative NLS. So far, two distinct classes of NLSs have been identified: a single stretch of basic residues, exemplified by the NLS of the simian virus 40 (SV40) large tumor/antigen, and two clusters of basic residues separated by a spacer region of 10–12 amino acids, as typified by *Xenopus laevis* nucleoplasmin.[9,10] These signals are usually recognized by the cytoplasmic receptor proteins Imp-α and Imp-β and actively translocated through the pore channel.[11,12] The directionality of nuclear import is thought to be conferred by the asymmetric distribution of the guanosine triphosphate– and guanosine diphosphate–bound forms of protein Ran between cytoplasm and nucleus.[13,14] The nuclear pore complex (NPC) also mediates passive bi-directional diffusion of proteins of molecular masses of up to 60–70 kd.[15]

So far, the mechanism directing the nuclear import of the Tat peptide has been studied only by *in vitro* assays, with contradictory results. Truant and Cullen proposed an active nuclear import mechanism involving cytosolic factors (Imp-β, but not Imp-α) and suggested the existence of a novel class of basic NLS sequences that function independently of Imp-α.[16] In contrast, Efthymiadis *et al.* reported that the Tat peptide can target a large heterologous protein (β-galactosidase from *Escherichia coli*, 120 kd) to the nucleus in the absence of both Imp-β and Imp-α. An entirely novel pathway was invoked that involves energy consumption and binding to nuclear components.[17]

In this work we chose a different approach that allowed us to investigate Tat peptide intracellular transport properties in living cells without the need to disrupt the integrity of the cytoplasmic or nuclear membranes. We designed green fluorescent protein (GFP)–based fusion proteins of different molecular sizes, both below and above the passive diffusion size limit. These constructs represent a benchmark for intracellular passive diffusion behavior

**Current address:* *International Centre for Genetic Engineering and Biotechnology, Padriciano, Trieste, Italy*
***Correspondence:** Francesco Cardarelli, Scuola Normale Superiore, Italian Institute of Technology, Piazza dei Cavalieri 7, I-56126 Pisa, Italy.*
E-mail: f.cardarelli@sns.it

when expressed in cells and were also used as cargoes for prototypical active import by fusing them to the NLS of SV40. The behavior of these two classes of constructs was compared with that of the same GFP cargoes fused to the Tat peptide. We analyzed the sub-cellular localization of all constructs by confocal imaging and addressed their intracellular dynamics using the fluorescence recovery after photobleaching (FRAP) method. Photobleaching is an irreversible photochemical change in the fluorophore structure so that it is no longer fluorescent. In a FRAP experiment, fluorescent molecules in a selected region of the cell are irreversibly photobleached using a high-power laser beam. The subsequent movement of surrounding non-bleached fluorescent molecules into the photobleached area is recorded at low laser power. Results from these experiments allow one to probe the trafficking properties of a given protein within living cells.[18]

We measured the characteristic kinetic parameters of Tat peptide intracellular dynamics and concluded that the molecular mechanism directing Tat peptide movement across the nuclear envelope (NE) is passive diffusion. Important limitations of this route in terms of acceptable cargo size are provided. We believe that the present results can be of great interest for those who exploit Tat peptide as a molecular carrier, to fine-tune its diagnostic and therapeutic efficacy.

RESULTS

Engineering, expression, and localization of constructs

To assess the nucleus/cytoplasm shuttling properties driven by the Tat peptide sequence we engineered three pcDNA3-based constructs encoding differently sized GFP-based cargoes.

We constructed a prototypical passive diffusion system composed of a small protein able to diffuse freely between nucleus and cytoplasm (single enhanced GFP, or EGFP) and a larger complex consisting of an enhanced blue fluorescent protein (EBFP) linked to an EGFP (hereafter, GFP_2) (**Figure 1a**). In addition, we studied a third fusion protein, consisting of a higher molecular weight (MW) cargo composed of E^1GFP (a mutated EGFP derivative), EGFP, and the dimeric red fluorescent protein tdTomato (hereafter, GFP_4) (**Figure 1a**), whose size makes it unable to diffuse across the NE.[20] GFPs were chosen because they are known not to interact with intracellular substrates and, in particular, not to contain an NLS capable of triggering active nuclear transport.[19]

Expression of the three different proteins and their correct size was verified by western blot analysis. As shown in **Figure 1b**, the single GFP protein shows an apparent mass of 27 kd, and GFP_2 and GFP_4 are detected at 56 and 110 kd, respectively. For this last construct, data indicate the presence of a detectable fraction of degraded fragments at lower MW, a result not unexpected in the case of such a complex system.

To examine intracellular distribution of these proteins in living cells, Chinese hamster ovary (CHO) K1 cells were transfected with the three constructs. After 20 hours, cells were incubated with the DNA-staining Hoechst dye for 30 minutes and then examined by confocal microscopy (**Figure 1c**). As expected for a purely diffusive molecule, GFP displayed a uniform distribution throughout the cell with no sub-cellular organelle-specific localization.[20] We obtained the same result in the case of GFP_2: the cytoplasm and the nucleus of cells were uniformly labeled by this protein. In contrast, GFP_4 was detected in the cytoplasm but excluded from the nuclear compartment in most of the cells analyzed, as expected from the expression of a 110-kd protein lacking an NLS. A small (~10%) fraction of the cells, however, showed detectable nuclear staining (data not shown) that can be linked to degradation fragments of the GFP_4 protein, as suggested by immunoblotting analysis (GFP_4 lane in **Figure 1b**).

To investigate the ability of Tat11 to mediate nuclear import of these cargoes, we obtained three additional constructs that expressed the three proteins with an additional N-terminal tag corresponding to the Tat11 peptide sequence (YGRKKRRQRRR).

Finally, a third set of constructs was produced by replacing the Tat11 sequence with the NLS of the SV40 T antigen (YPKKKRKVEDP). This set provides our active import benchmark. A multiple site-directed mutagenesis was performed to replace the selected single amino acids of the Tat11 sequence with the residues belonging to the NLS_{SV40} sequence, as indicated in **Figure 1a**.

Cargo-dependent sub-cellular localization of constructs

As a first test, we transfected CHO K1 cells with Tat11-tagged GFP, GFP_2, and GFP_4 cargoes and analyzed their sub-cellular distribution

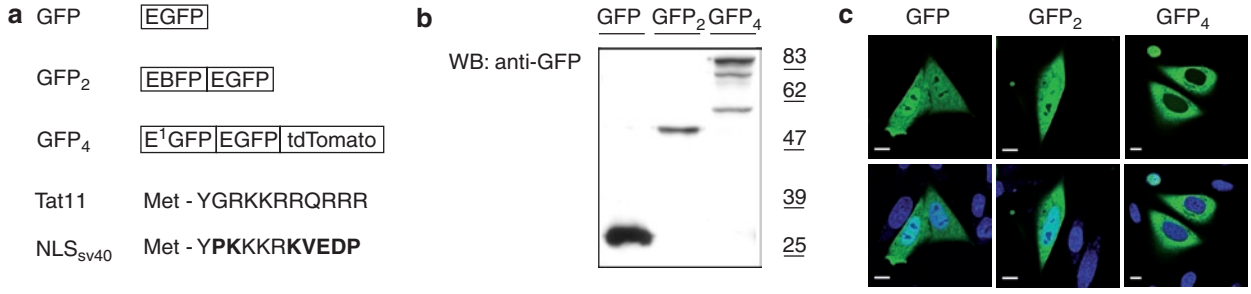

Figure 1 Engineering, expression, and localization of constructs. (**a**) Schematic representation of cargo construct composition (green fluorescent protein (GFP, GFP_2, and GFP_4)). Tat11 and nuclear localization signal of the simian virus 40 (NLS_{SV40}) sequences are represented by single-letter amino acid code (residues obtained by mutagenesis are highlighted in bold type). (**b**) Total cellular proteins (10 μg) obtained from transfection of GFP, GFP_2, and GFP_4 expression vectors in Chinese hamster ovary K1 cells were analyzed by sodium dodecyl sulfate polyacrylamide gel electrophoresis and immunoblotted with an anti-GFP monoclonal antibody to highlight the correct molecular weight of cargoes. (**c**) Confocal images of expressed cargo proteins (upper panels); the same images superimposed to Hoechst dye nuclear stain (lower panels). Scale bar: 10 μm. EBFP, enhanced blue fluorescent protein; EGFP, enhanced GFP; E^1GFP, a mutated EGFP derivative.

using a confocal microscope. Independent of the level of transfection, Tat11-GFP sub-cellular distribution was relatively uniform between cytoplasm and nucleoplasm (K_{eq} = nuclear concentration/cytoplasmic concentration ~ 1; "B" in **Table 1**), with a concomitant detectable enrichment in nucleolar fluorescence (**Figure 2a**). In an analogous manner, Tat11-GFP_2 preserved the homogeneous distribution between nucleus and cytoplasm (**Figure 2b**). Remarkably, Tat11-GFP_4 was almost exclusively localized within the cytoplasm of expressing cells (**Figure 2c**), indicating that the Tat11 sequence was not able to mediate the nuclear import of a cargo that is above the limit for passive diffusion across the NPC. In short, the cargo-dependent sub-cellular localization of Tat11-based constructs closely resembles that of their corresponding passive diffusion benchmarks discussed above (**Figure 1c**). The actual size of the GFP and Tat11-GFP constructs was verified by western blot analysis using an anti-GFP monoclonal antibody. Two lanes were detected at different positions in the gel, consistent with a ~1.5-kd mass difference (data not shown).

Table 1 Transport parameters derived from nuclear FRAP measurements

Row	Protein	K_{eq}	$\tau_{C\to N}$ (s)	D/W (μm³/s)	*N*
A	GFP	~1	77 ± 19	13.6 ± 3.7	24
B	Tat11-GFP	~1	410 ± 125	2.7 ± 1.5	39
C	NLS_{SV40}-GFP	2.2–4.4	60 ± 3	5.2 ± 0.6	14
D	GFP_2	~1	1178 ± 292	1.13 ± 0.5	8
E	Tat11-GFP_2	~1	1165 ± 305	1.2 ± 0.4	5
F	NLS_{SV40}-GFP_2	8–22	240 ± 57	0.8 ± 0.3	13
G	NLS_{SV40}-GFP_4	24–56	ND	ND	ND

Abbreviations: D/W passive diffusion parameter (mean ± SD values, defined in Materials and Methods and Results); GFP, green fluorescent protein; K_{eq}, ratio between nucleoplasmic and cytoplasmic fluorescence (range of reported values); *N*, number of cells examined; ND, no data; NLS_{SV40}, nuclear localization signal of the simian virus 40; $\tau_{C\to N}$, time constant of nuclear fluorescence recovery (mean ± SD values).

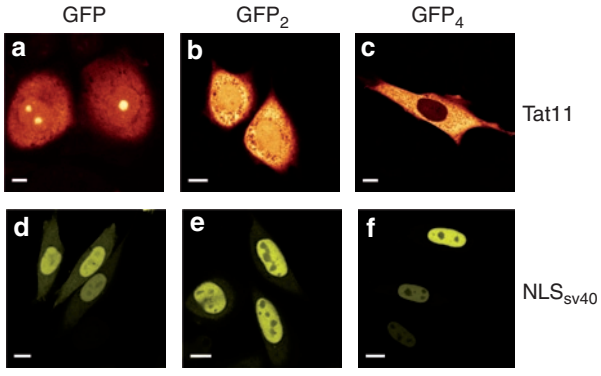

Figure 2 Cargo-dependent sub-cellular localization. Sub-cellular localization of Tat-tagged cargoes imaged by confocal microscopy: (**a**) Tat11-green fluorescent protein (Tat11-GFP) and (**b**) Tat11-GFP_2 are uniformly distributed between compartments (cargo molecular weight (MW) is under the limit for passive diffusion), whereas (**c**) Tat11-GFP_4 is excluded from the nucleus (cargo MW above the limit for passive diffusion). In contrast, nuclear localization signal of the simian virus 40 (NLS_{SV40})–tagged cargoes are predominantly localized in the nucleus of expressing cells. In particular, the nuclear accumulation of these constructs is proportional to the increasing MW of the cargo (compare sub-cellular localizations in **d**–**f**). In fact, these proteins are actively and rapidly imported by specific carriers, and their nucleus-to-cytoplasm passive diffusion is progressively impaired.

Finally, we analyzed the sub-cellular localization of NLS_{SV40}-tagged constructs. A markedly different behavior was observed (**Figure 2**, lower panels). In this case, all GFP cargoes were successfully imported and, consequently, under physiological conditions, were predominantly detected in the nucleus (K_{eq} > 1, "C," "F," and "G" in **Table 1**). It is worth noting that nuclear accumulation of NLS_{SV40}-based constructs was even more marked with increasing cargo MW (compare sub-cellular localizations in **Figure 2d–f**). This peculiar behavior can be linked to the fact that although both large and small proteins are rapidly imported owing to the NLS-specific active processes, their nucleus-to-cytoplasm passive diffusion is impaired by the increasing cargo size.

Nuclear permeation upon energy depletion

Selectively to monitor the role of active processes in determining the nuclear permeation of the proteins tested, we analyzed their sub-cellular localization in response to energy depletion. Intracellular adenosine triphosphate/guanosine triphosphate stores were depleted by incubating cells with 2-deoxy-D-glucose and sodium azide in glucose-free medium. Within 30 minutes of this treatment, most cells lost Mitotracker staining (**Figure 3k** and **l**), indicating that their mitochondria were no longer active.[21,22] We found that when cells expressing NLS_{SV40}-GFP were incubated in the energy depletion medium, fluorescence rapidly equilibrated between nucleus and cytoplasm (**Figure 3b**). This behavior is

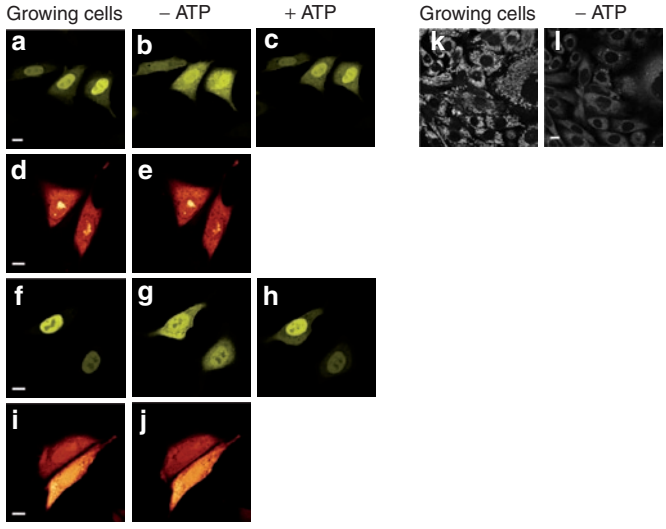

Figure 3 Nuclear permeation on energy depletion. (**a**) The functional nuclear localization signal (NLS) of simian virus 40 is able to accumulate green fluorescent protein (GFP) cargo into the nucleus under physiological conditions (growing cells). (**b**) After 30 minutes of energy depletion treatment, NLS_{SV40}-GFP equilibrated between nucleus and cytoplasm (–ATP). (**c**) Within 10–15 minutes after shifting the same cell back to physiological conditions, active nuclear import was restored (+ATP). (**d, e**) Similar energy depletion assays did not alter the sub-cellular localization of Tat11-GFP. Scale bar: 10 μm. (**f–h**) Accordingly, we observed that NLS_{SV40}-GFP_2 localization was reversibly modulated by energy depletion assay, (**i, j**) While Tat11-GFP_2 localization was not altered by the same treatment Scale bar: 10 μm. (**k**) Under physiological conditions, Mitotracker is selectively sequestered by active mitochondria. (**l**) Within 30 minutes after treatment with 2-deoxy-D-glucose and sodium azide, a 60–70% decrease in Mitotracker staining is observed, indicating mitochondrial failure. Scale bar: 10 μm. ATP, adenosine triphosphate.

consistent with the dominant NLS-mediated nuclear import: when the latter is blocked by energy depletion, NLS_{SV40}-GFP passive diffusion to the cytoplasm can successfully restore a homogeneous intracellular distribution. Notably, this behavior is reversible: within a few minutes of shifting cells back to physiological conditions, fluorescence was again predominantly localized in the nucleus (**Figure 3c**). The same treatment showed no effect on Tat11-GFP sub-cellular localization (**Figure 3d** and **e**), providing the first evidence that Tat11-driven cargo trafficking is an energy-independent mechanism.

We performed analogous measurements on NLS_{SV40}-GFP_2 and Tat11-GFP_2. As shown in **Figure 3f–h**, NLS_{SV40}-GFP_2 equilibrated between nucleus and cytoplasm under energy depletion conditions and promptly accumulated in the nucleus when active import was restored. Once again, however, the same treatment showed no effect on Tat11-GFP_2 sub-cellular localization (**Figure 3i** and **j**). Analogously to Tat peptide constructs, isolated GFP and GFP_2 showed no energy-dependent sub-cellular distribution (data not shown), as expected for these passive diffusion benchmark proteins. Comparing the behaviors displayed by Tat11 constructs and the two benchmarks provides a further indication of a dominant passive diffusion mechanism for the Tat peptide across the NE.

Dynamic model for nuclear/cytoplasmic exchange

We addressed the quantitative aspects of the nuclear/cytoplasm exchange by means of a set of time-resolved experiments analyzed using a dynamic model that includes both reversible passive diffusion between the two compartments and active nuclear import of proteins from the cytoplasm (**Supplementary Figure S1**). The passive diffusion flux plays a role in the case of proteins that are characterized by an MW less than the nuclear pore exclusion limit. Active transport flux must be included when NLS properties need be included. We did not include nucleus-to-cytoplasm active transport processes in our dynamic model. Each contribution is characterized by one transport parameter: D/W for passive diffusion and v^0/C_C^0 for active transport. It is worth noting that D/W is a purely dynamic parameter, specific to the diffusing protein, whereas v^0/C_C^0 depends both on the NLS-induced nuclear import rate (v^0) and on the expression level in the cytoplasm (C_C^0). These parameters can be experimentally determined by studying the FRAP of nuclear and cytoplasmic compartments.

FRAP analysis of nucleus/cytoplasm exchange: passive diffusion

Constructs encoding for untagged GFP proteins were investigated first to provide the passive diffusion benchmark parameters. The fluorescence of the nuclear compartment of CHO K1 cells transiently transfected with GFP was photobleached by irradiating a single point with high laser power for 8 seconds. The subsequent fluorescence recovery was recorded by time-lapse acquisition at 20-second intervals (**Figure 4a**). As photobleaching is an irreversible process, the fluorescence recovery in the nucleus is attributable to the influx of unbleached GFP molecules from the cytoplasm, in equilibrium with the efflux of bleached molecules from nucleus to cytoplasm (compare green curves on open and filled circles in **Figure 4e**). Indeed, the fluorescence in the

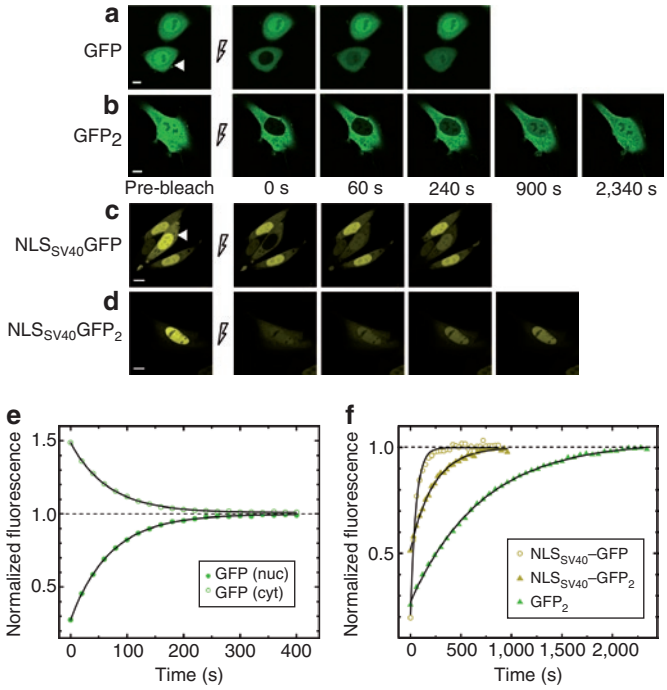

Figure 4 ***In vivo*** **fluorescence recovery after photobleaching (FRAP) analysis of reversible passive diffusion and active nuclear import.** (**a**) Fluorescence recovery after nuclear photobleaching as green fluorescent protein (GFP) diffuses from cytoplasm to nucleus. Nuclear fluorescence (pre-bleaching panel, white arrow) was photobleached by irradiating a single point with high laser power for 8 seconds. Recovery was recorded by time-lapse imaging: selected images are reproduced, with the corresponding time of acquisition. Scale bar: 10 μm. (**b**) As in **a**, FRAP analysis of nucleus/cytoplasm exchange of GFP_2 (16-second single-point bleaching). Scale bar: 10 μm. (**c**) FRAP analysis of actively imported nuclear localization signal of the simian virus 40 GFP (NLS_{SV40}-GFP). Nuclear fluorescence (pre-bleaching panel) was photobleached by irradiating a single point with high laser power for 10 seconds, and subsequent recovery was monitored by time-lapse imaging: selected images are reproduced, with the corresponding time of acquisition. Scale bar: 10 μm. (**d**) As in **c**, FRAP analysis of actively imported NLS_{SV40}-GFP_2 (18-second single-point bleaching). The intensity of post-bleaching images has been adjusted to show the fluorescence recovery signal better. (**e**) Time course of nucleoplasmic fluorescence recovery (filled green circles) for the cell shown in **a**. Cytoplasmic fluorescence concomitantly decreases as GFP diffuses from cytoplasm to nucleus (open green circles). This symmetric process shows the same kinetics, yielding a time constant (τ) of approximately 70 seconds for the analyzed cell (single-exponential fits are represented by continuous black lines). Both FRAP curves are normalized by pre-bleaching values: the asymptotic value of 1 indicates that no immobile fraction of molecules can be detected in the bleached compartment (the nucleus). (**f**) Kinetics of nucleoplasmic fluorescence recovery after photobleaching for cells shown in **b**–**d**. τ-values (mean ± SD) are 704 ± 8 seconds (GFP_2, green triangles), 230 ± 5 seconds (NLS_{SV40}-GFP_2, yellow triangles), 54 ± 2 seconds (NLS_{SV40}-GFP, open yellow circles). As in **e**, the asymptotic value of 1 of recovery curves indicates that no immobile fraction of molecules is present in the nuclear compartment. Transport parameters for the whole population of analyzed cells are reported in **Table 1**.

cytoplasm decreased as GFP diffused from cytoplasm into the nucleus. As expected, after cytoplasm photobleaching, cytoplasm fluorescence recovered concomitantly with a decrease in nuclear fluorescence (**Supplementary Figure S2**). Consistent with the hypothesis of an effective nucleus/cytoplasm exchange, the kinetic characteristics of cytoplasm fluorescence recovery resembled those of the nucleus (data not shown). Also, as we are dealing

with restricted exchange between two well-mixed compartments (the nucleus and the cytoplasm) and the boundary properties (*i.e.,* the permeability properties of the nuclear membrane owing to the finite number of nuclear pores) mostly influence the diffusive recovery kinetics, the post-bleaching concentration dynamics is described by exponential decays.[23,24] Indeed, the kinetics of fluorescence recovery in all measured cells was accurately fitted by a single exponential function (fit errors were always found to be in the range 1–5%) whose time constant (τ) expresses the rate of the protein shuttling across the nuclear membrane.

Results from the whole population of analyzed cells yielded a τ-value of 77 ± 19 seconds ("A" in **Table 1**) for GFP shuttling. All recovery curves were normalized taking into account the pre-bleaching fluorescence values, to estimate the amount of immobile fraction within the bleached compartment. The asymptotic value of 1 in **Figure 4e** and **f** indicates that the pool of nuclear proteins was completely exchangeable with the cytoplasm, as expected for a protein that does not interact with any sub-cellular substrates. These findings are in agreement with published data addressing GFP passive bi-directional diffusion across the nuclear membrane.[20]

We performed analogous FRAP measurements to evaluate nucleus/cytoplasm shuttling of isolated GFP_2 in the same conditions (**Figures 4b** and **f**). Nuclear fluorescence was photobleached by irradiating for 16 seconds a single point with high laser power. The subsequent recovery was monitored by time-lapse imaging at 60-second intervals. We obtained an overall τ-value of 1,178 ± 292 seconds ("D" in **Table 1**). This slower recovery rate of passively diffusing GFP_2 (compared with GFP) is expected, as its MW is close to the estimated molecular cut-off size for passive diffusion through the NPC (*i.e.,* ~60–70 kd)[25,26] and is in good agreement with recently reported *in vivo* analyses.[27] Cytoplasmic FRAP measurements yielded almost identical recovery rates (data not shown), providing additional evidence of symmetric nucleus/cytoplasm shuttling. As for the case of single-GFP cargo, we reported no detectable immobile fraction of fluorescent proteins in the bleached compartment.

Our dynamic model allowed us to calculate the characteristic diffusion parameters (D/W) of GFP benchmarks. The D/W value for GFP is more than 10 times that for GFP_2 ("A" and "D" in **Table 1**) as a consequence of the reported shuttling time constants. In both cases, the concentration of the diffusing proteins in the nucleoplasm and the cytoplasm was the same before bleaching and asymptotic after bleaching ($K_{eq} = 1$). On the basis of our kinetic analysis (see Equation [7] in **Supplementary Materials and Methods**), we can conclude that no active nuclear import contribution was detectable ($v^0/C_C^0 = 0\,\mu m^3/s$).

FRAP analysis of nucleus/cytoplasm exchange: active import

We quantitatively investigated NLS_{SV40}-driven transport to determine the rates of active import compared with passive diffusion. NLS_{SV40}-GFP nuclear fluorescence was photobleached by irradiating for 10 seconds a single point with high laser power. The subsequent recovery was monitored by time-lapse imaging at 30-second intervals (**Figure 4c**). **Figure 4f** shows the nuclear fluorescence recovery data of NLS_{SV40}-GFP (open yellow circles) and the corresponding single-exponential fit. From the kinetic analysis of the whole FRAP dataset we found that active nuclear import is characterized by a recovery time constant of 60 ± 3 seconds ("C" in **Table 1**). From the whole population of cells examined we derived a characteristic v^0/C_C^0 value of 10 ± 4.5 $\mu m^3/s$ for NLS_{SV40}-GFP active import and a D/W value of 5.2 ± 0.6 seconds for its concomitant reversible passive diffusion ("C" in **Table 1**).

As for the case of single-GFP cargoes, we tested the influence of molecular size on the NLS-driven nuclear import kinetics. To this end we performed FRAP analysis of NLS_{SV40}-GFP_2. Nuclear fluorescence was photobleached by 18-second single-point irradiation with high laser power, and the subsequent recovery was monitored by time-lapse imaging at 30-second intervals (**Figure 4d**). NLS_{SV40}-GFP_2 active import is approximately five times faster than isolated GFP_2 shuttling across NE (**Figure 4f**). Overall τ-values are reported in "D" and "F" in **Table 1**. By means of our kinetic model we calculated a v^0/C_C^0 value of 8.2 ± 3 $\mu m^3/s$, revealing that active import is not much affected by a twofold increase in cargo size. Reversible passive diffusion was slowed down by NPC restriction (D/W parameters in "F" in **Table 1**).

FRAP analysis of Tat11-cargoes: nucleus/cytoplasm exchange

Having set the benchmark values for purely diffusive and active transport–dominated constructs, we established nucleus/cytoplasm exchange parameters for Tat11-tagged cargoes. The sub-cellular localization of Tat11-tagged proteins is not that typical of the NLS-tagged ones, and this makes it possible to investigate the behavior only of constructs that are below the passive diffusion limit (*i.e.,* Tat11-GFP and Tat11-GFP_2).

For Tat11-GFP, we must take into account its observed nucleolar accumulation. In this case, nuclear fluorescence recovery kinetics is the result of two distinct processes: Tat11-GFP transfer across the NE and its nucleolus/nucleoplasm exchange. We found that communication between nucleoplasm and nucleolus takes place on a much shorter time-scale than shuttling across the NE. In fact, nucleolar fluorescence reaches its plateau value approximately 8 seconds after photobleaching (**Supplementary Figure S3**). As we are interested mainly in the much slower nucleus/cytoplasm shuttling of Tat11-GFP, we neglected nucleolar kinetics in the analysis of FRAP data.

The fluorescence of the nuclear compartment was photobleached by irradiating for 30 seconds a single point with high laser power. The subsequent recovery was recorded by time-lapse acquisition at 30-second intervals (**Figure 5a**). We obtained $\tau = 410$ ± 125 seconds ("B" in **Table 1**). Tat11-GFP shuttles between nucleus and cytoplasm significantly more slowly than GFP alone (compare recovery curves in **Figure 5c** and τ-values with "A" and "B" in **Table 1**). Accordingly, the characteristic dynamic parameter D/W for Tat11-GFP is five times smaller than that of isolated GFPs ("A" and "B" in **Table 1**). No immobile fraction was detected (see **Figure 5c** and the asymptotic fluorescence recovery value of 1). Addition of inhibitors of proteolysis such as chloroquine and MG132 did not change Tat11-GFP sub-cellular distribution and inter-compartment dynamics, indicating that the fusion protein is insensitive to the main pathways of intracellular

degradation.[28,29] It is also worth noting that FRAP analysis of Tat11-GFP and GFP in transiently transfected HeLa cells yielded analogous results (data not shown), providing evidence that our data are not determined by the specific cell line chosen.

The large increase of the shuttling time constant induced by Tat11 fusion cannot be attributed to the effect of the increase in MW attributable to the peptide on the passive diffusion properties of GFP, as Tat11-GFP is only approximately 1.5 kd larger than isolated GFP. These results and the observed marked nucleolar staining of Tat11-GFP suggest that the ability of this construct to interact with cellular molecular components must be taken into account. We further address this issue by investigating the impact of Tat11 on the intra-compartment diffusion properties.

In the case of Tat11-GFP$_2$ shuttling, nuclear fluorescence was photobleached by irradiating a single point with high laser power for 30 seconds. Signal recovery was then monitored by time-lapse imaging at 60-second intervals (**Figure 5b**). We obtained an overall τ-value of 1,165 ± 305 seconds ("E" in **Table 1**). Note that, within experimental error, this value coincides with that of isolated GFP$_2$. This is not surprising in light of the impact of Tat11 fusion to the smaller construct: the addition of Tat11 led to a modification of the measured shuttling constant, which is a rather small fraction of the isolated GFP$_2$ τ-value, actually within the estimated experimental error. Also in this case we adopted the usual normalization procedure, and the observed asymptotic value of 1 for nuclear fluorescence recovery reveals that (just as for GFP$_2$ alone) the Tat11-GFP$_2$ population is fully exchangeable between compartments (**Figure 5c**). Our dynamic model yielded approximately the same D/W value for the two species ("D" and "E" in **Table 1**). Notably, as for isolated GFP$_2$, we found no detectable contribution of any active transport mechanism ($v^0/C_C^0 = 0\,\mu m^3/s$). These results are fully consistent with the previous observations and once again point toward the diffusive nature of Tat11-GFP$_2$ trafficking.

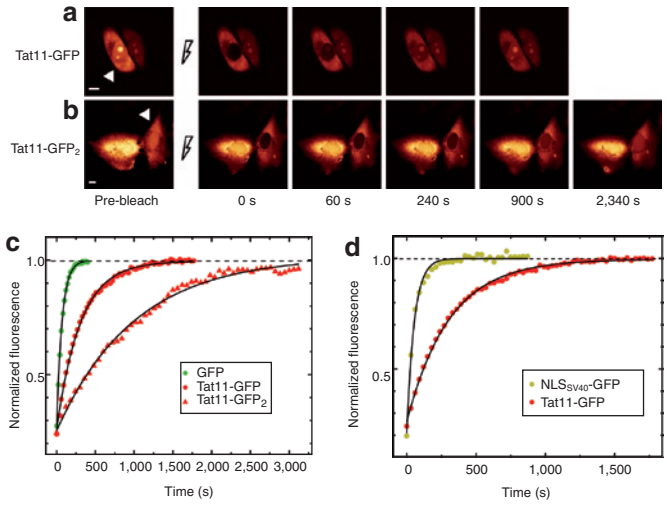

Figure 5 ***In vivo*** **fluorescence recovery after photobleaching (FRAP) analysis of nucleus/cytoplasm Tat11 cargo shuttling.** (**a**) Fluorescence recovery after nuclear photobleaching as Tat11-green fluorescent protein (Tat11-GFP) diffuses from cytoplasm to nucleus. Nuclear fluorescence (pre-bleaching panel, white arrow) was photobleached by irradiating a single point with high laser power for 30 seconds. Recovery was recorded by time-lapse imaging: selected images are reproduced, with the corresponding time of acquisition. Scale bar: 10 μm. (**b**) As in **a**, FRAP analysis of Tat11-GFP$_2$ shuttling (white arrow, 30-second single-point bleach). Scale bar: 10 μm. (**c**) Kinetics of nucleoplasmic FRAP for cells shown in **a** and **b** compared with the GFP recovery curve from **Figure 4e**. τ-values (mean ± SD) are 70 ± 0.5 seconds (GFP, green circles), 307 ± 4 seconds (Tat11-GFP, red circles), 1,006 ± 34 seconds (Tat11-GFP$_2$, red triangles). All FRAP curves are normalized by pre-bleaching values; the asymptotic value of 1 indicates that no immobile fraction of molecules is present in the nuclear compartment. Transport parameters for the whole population of analyzed cells are reported in **Table 1**. (**d**) Tat11-GFP recovery curve (red circles, already shown in **c**) is here compared with the faster active import kinetics of the corresponding nuclear localization signal of the simian virus 40 GFP (NLS$_{SV40}$-GFP) benchmark (yellow circles, already shown in **Figure 4f**).

FRAP analysis of protein mobility within cytoplasm

The previous section showed the impact of Tat11 on the nucleus/cytoplasm shuttling and provided strong indications of the relevance of Tat peptide interactions in determining the overall construct properties. For example, it is well known that arginine-rich motifs strongly interact with RNA molecules,[30,31] but other molecules may play a significant role. To isolate the impact of these interactions from NE crossing, we investigated the intra-cytoplasm diffusion properties of our constructs. As usual, we used isolated GFPs as benchmarks, as it is well known that these proteins have no interactions with sub-cellular substrates. In these experiments we bleached a small region (≈7 μm diameter) of the cytoplasm

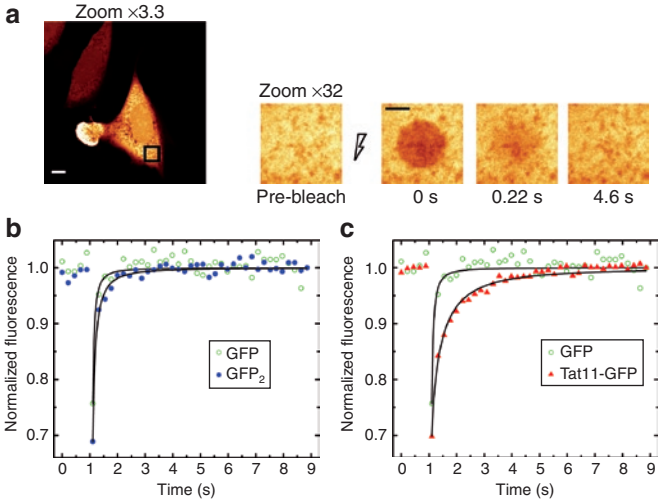

Figure 6 **Protein mobility within cytoplasm: bleaching of a uniform disk.** (**a**) An image of the whole cell was recorded to monitor the fluorescence signal before bleaching (zoom ×3.3 panel; scale bar: 10 μm). A selected region within cytoplasm (dark square) was then imaged (zoom ×32 panel; scale bar: 3.5 μm) and a circular area of 3.5-μm radius was photobleached using 476-, 488-, and 514-nm light at maximum power. Fluorescence recovery was then monitored at 220-millisecond intervals for approximately 8 seconds using 488-nm excitation at low power: selected images are reproduced with the corresponding time of acquisition. (**b**) Characteristic recovery curves of green fluorescent protein (GFP) (open circles) and GFP$_2$ (filled circles). Data are normalized as described in the text; the asymptotic value of 1 reveals that no immobile fraction is present in the cytoplasmic bleached region. Fitting to Equation [3] (solid black lines) yielded the D values of 19 ± 4 μm^2/s for GFP and 14.3 ± 1.5 μm^2/s for GFP$_2$ (mean ± SD values). Diffusional parameter analysis of the whole population of examined cells is reported in **Table 2**. (**c**) Characteristic recovery curve of Tat11-GFP (filled triangles, D = 3.9 ± 0.2 μm^2/s) compared with GFP (open circles, D = 19 ± 4 μm^2/s). Overall statistics are reported in **Table 2**.

Table 2 Diffusion parameters derived from cytoplasmic FRAP measurements

Row	Protein	D (μm²/s)	K_0	N
A	GFP	20 ± 5	0.67 ± 0.17	39
B	Tat11-GFP	5.9 ± 1.5	0.68 ± 0.17	31
C	GFP_2	13.8 ± 5.5	0.61 ± 0.11	50
D	Tat11-GFP_2	4 ± 1	0.72 ± 0.07	19

Abbreviations: *D*, effective diffusion coefficient within cytoplasm (mean ± SD values); GFP, green fluorescent protein; K_0, bleaching parameter (mean ± SD values); *N*, number of cells examined.

by irradiation with a 220-millisecond high-intensity laser pulse and monitored the recovery process by fast time-lapse imaging (**Figure 6a**). The speed of recovery of fluorescence is correlated to the mobility of the fluorescent reporter, with a faster time course being associated with a larger diffusion coefficient.[18] Fluorescence recovery in all the measured cells was accurately described by Equation [3] (solid lines in **Figure 6b** and **c**). We derived the effective diffusion coefficient (D) of the molecule in cytoplasm and the value of the bleaching parameter K_0 (related to the bleaching depth) for all the proteins tested. Note that the K_0 value is approximately the same for all the proteins tested (**Table 2**), as expected for a parameter that depends only on the nature of the fluorophore (GFP) and the experimental parameters adopted (unchanged in the cytoplasmic FRAP measurements).[43]

We obtained $D = 20 \pm 5\,\mu m^2/s$ for GFP and $D = 13.8 \pm 5.5$ for GFP_2 ("A" and "C" in **Table 2**). These values are in agreement with previously reported data for GFP diffusion in CHO cell cytoplasm[32] and for both GFP monomer and dimer diffusion in COS-1 cell cytoplasm.[27]

The fusion with Tat11 significantly changes the diffusivity. We obtained $D = 5.9 \pm 1.5\,\mu m^2/s$ ("B" in **Table 2**) for Tat11-GFP and $D = 4 \pm 1\,\mu m^2/s$ for Tat11-GFP_2 ("D" in **Table 2**).

This large change far exceeds what could be induced by the simple addition of 1.5 kd and confirms the previous indication that fusion with Tat11 leads to increased interactions. Note, however, that Tat peptide is not immobilized within the cytoplasm, as we measured a complete fluorescence recovery after bleaching of a uniform disk (**Figure 6c**).

DISCUSSION

In this work we addressed the intracellular dynamics of intact Tat peptide cargoes in living cells by means of FRAP analysis. The mechanism of Tat peptide–driven nuclear permeation was identified, together with the potential and the limitations of Tat as a molecular carrier from the point of view of cargo size. These results complement the large number of studies that investigate Tat as a vehicle for trans-cellular protein delivery. These latter studies indicate that the conjugation of non-permeant molecules to the Tat peptide allows their cellular uptake and can lead to the desired biological response, consistent with peptide cargoes actually reaching the cytosol intact and with their full biological functionality.

The sub-cellular localization of expressed Tat11-based constructs was first investigated and compared with the corresponding passive diffusion and active import benchmarks: isolated GFPs and NLS_{SV40}-tagged constructs, respectively (**Figure 2**). Tat11-tagged proteins showed unambiguously the same localization as their passive diffusion counterparts. In particular, Tat11-GFP_4 with a cargo above the diffusion limit was excluded from the nucleus, revealing that Tat peptide is not able to transport large cargoes to this compartment. In contrast, the functional NLS of SV40 displayed nuclear localization of cargo proteins. Tat11 behavior is consequently not consistent with the assumption that active transport is the dominant nuclear localization mechanism of the peptide. We then tested the hypothesis that passive diffusion might be the dominant mechanism in our experiments by analyzing the influence of energy depletion. In fact, adenosine triphosphate is required for the active transport mechanism, as shown for the case both of intact cells and of cell-free systems.[33,34] Also for this test, we used NLS_{SV40}-tagged constructs as benchmarks for active import from the cytoplasm into the nucleus. It is worth noting that the models so far proposed, including for the present case, of Tat peptide–mediated nuclear import do demand metabolic energy in the form of adenosine triphosphate, independent of the specific molecular model proposed.[16,17] Our data show that NLS_{SV40}-GFP (and NLS_{SV40}-GFP_2) were not imported into the nucleus upon energy depletion, whereas Tat11-GFP (and Tat11-GFP_2) sub-cellular localization was not affected by the same treatment (*i.e.*, re-localization was not observed) (**Figure 3a**). Taken together, these findings lead to the conclusion that the mechanism underlying Tat11 nuclear permeation is passive diffusion. This is in contrast with previously reported *in vitro* studies that have highlighted the relevance of active processes in Tat peptide–driven nuclear import[16,17] and prompted us to consider the detailed experimental conditions of these studies. In particular, we believe that the impact of the non-physiological conditions characteristic of import assays in permeabilized cells should be carefully evaluated. For example, one important issue in such experiments is the absence of co-factors that can influence Tat peptide properties. Specifically, although we cannot exclude the idea that Imp-β may be one interacting partner of Tat peptide, our data demonstrate that, if at all present, this interaction does not lead to a detectable energy-dependent route of nuclear import. A likely explanation is that the interaction between Imp-β (or any other suitable carrier) and Tat peptide is efficiently inhibited by other cellular substrate molecules such as RNAs. Indeed Friedler *et al.* reported a strong inhibition of Tat peptide nuclear import by the addition of cytosolic factors (including RNA and Imp-α)[35] that usually leak out of the cells during cell permeabilization. It is well established that arginine-rich sequences strongly interact with RNA molecules. For instance, it has been demonstrated that continued ribosomal RNA synthesis is involved in Rev nucleolar accumulation.[36] Moreover, it was shown that the arginine-rich sequence of Rev has a much higher affinity for RNA molecules than it does for the Importins[36] and that cellular RNAs are able efficiently to block its Imp-β nuclear import.[38] We conclude that our *in vivo* assays that largely preserve physiological interactions of the Tat peptide show that Tat peptide properties are not dominated by interaction with import carriers.

Once we had established that passive diffusion dominates Tat11 cargo trafficking, we quantitatively defined the transport parameters of this route and investigated the limitations of Tat11 peptide as a molecular carrier from the point of view of size and type of acceptable cargo molecule. We addressed this point by

in vivo FRAP analysis. The real-time dynamics between nucleus and cytoplasm of passive diffusion and active import benchmark proteins was first investigated (**Figure 4**). By irreversibly photobleaching the protein within one compartment and measuring the rate of fluorescence recovery, we found that active import is faster than passive diffusion (see τ-values in **Table 1**). This effect is particularly evident for NLS_{SV40}-GFP_2: despite a twofold increase in cargo size, its active import time constant is approximately five times smaller than that of the corresponding passive diffusion dynamics of isolated GFP_2.

FRAP analysis of Tat11-GFP and Tat11-GFP_2 revealed that these proteins shuttle bi-directionally between the two compartments, with the same values applying to cytoplasm-to-nucleus transfer (signal recovery after nuclear photobleaching) and nucleus-to-cytoplasm transfer (signal recovery after cytoplasm photobleaching) (**Figure 5**). We must underline that this symmetry is in line with our conclusion that passive diffusion governs Tat11 cargo inter-compartment trafficking. For the case of Tat11-GFP, in particular, Tat11 fusion led to the observation of a sizable increase in τ-values (from 77 ± 19 to 410 ± 125 seconds). We have already argued that this increase cannot be attributed to the increase in MW brought about by the peptide on the passive diffusion properties of GFP, as Tat11-GFP is only approximately 1.5 kd larger than isolated GFP. These results once again must be linked to the ability of Tat peptide to interact with cellular molecular components. The impact of these interactions is not apparent in the case of GFP_2 constructs because of the large τ-value for the isolated GFP_2, determined by its size. We were able better to isolate the impact of Tat11 fusion for both constructs by investigating the effect of Tat11 on the intra-compartment diffusion properties. This was performed by photobleaching proteins within defined cytoplasm regions and monitoring the recovery process (**Figure 6**). Consistent with our conclusion of important Tat peptide–induced interactions, the Tat peptide sequence was shown to reduce the measured diffusion coefficients for both cargoes (for GFP: from 20 to 5.9; for GFP_2: from 13.8 to 4.0). No immobile fraction was observed. Taken together, these data indicate that the Tat peptide can significantly reduce intra-cytoplasm mobility much beyond the effect of its own size owing to its molecular interactions with cellular substrates (*e.g.,* RNA).

Our results provide useful insight into the nature of target molecules available for Tat peptide–driven nuclear delivery. First, our analysis shows that protein cargoes exceeding the size-threshold value for passive diffusion through the NPC will not gain access to the nuclear compartment. This is confirmed by the data published by Nitin *et al.*[39] These authors reported evidence that a Tat peptide–linked molecular beacon containing streptavidin is efficiently targeted to the cell cytoplasm but substantially excluded from the nucleus.[39] Moreover, results reported by Neumann *et al.* show that peptides containing the relevant Rev and Tat motifs conjugated with fluorescently labeled bovine serum albumin (66 kd) are not able to perform nuclear import upon cytoplasmic microinjection, in contrast to the nuclear accumulation observed using the NLS of SV40.[40]

Nonetheless, it must be noted that molecular cargoes up to 55 kd (namely, the size of GFP_2) can successfully reach the nucleus through the passive route unveiled here. Even though the emerging picture of the Tat peptide passive diffusion route demands a re-evaluation of the nature and size of acceptable target biomolecules for delivery purposes, we believe that significant areas of application do exist and that these limitations can be overcome by rational analysis and engineering of peptide structure.

MATERIALS AND METHODS

Construction of expression vectors. The expression vector encoding for EGFP protein was generated by polymerase chain reaction (PCR) amplification of EGFP template (pEGFP N1, Clontech, Mountain View, CA). Primers were all purchased from Sigma-Genosys (St. Louis, MO) and was inserted into *Hind*III–*Eco*RI sites of pcDNA3.1(+) vector from Invitrogen (Carlsbad, CA). For the construction of the plasmid encoding for EBFP-EGFP proteins, a first fragment generated from PCR amplification of EBFP template (p-EBFP C1 Clontech, Mountain View, CA) was inserted into *Hind*III–*Bam*HI sites of pcDNA3.1(+) vector. The second EGFP was cloned by two steps of PCR amplification into *Bam*HI and *Xba*I sites, introducing a spacer linker of 17 amino acids (ASGGGGGLVPR GSASGA) between the two EGFP sequences. The template used for PCR derived from p-EGFP N1 by Clontech.

To obtain the construct p-E^{1}GFP-EGFP-tdTomato, the E^{1}GFP template (an EGFP containing the mutations T65S T203Y) was inserted into *Hind*III and *Bam*HI sites of pcDNA3.1(+) including a streptavidin tag (MASWSHPQFEKGA) at the amino-terminal of the E^{1}GFP. A second EGFP (template p-EGFP N1 Clontech) was introduced by PCR amplification in *Bam*HI and *Eco*RI sites. Finally, the tdTomato template, obtained from Roger Y. Tsien's laboratory,[41] was amplified by PCR introducing an *Eco*RI site in the 5′ and an *Xba*I site in the 3′ extremity.

Constructs with Tat11 sequence used in this study were based on the Tat11-EGFP sequence cloned in pGEX2T plasmids described by Ferrari *et al.*[42] The fragment encoding for Tat11-EGFP protein was cut by *Bam*HI and *Eco*RI and sub-cloned in pcDNA3.0 vector (Invitrogen, Carlsbad, CA). Subsequently, a *Hind*III restriction site in the multiple cloning site was destroyed by mutagenesis using the QuickChange Kit (Stratagene, La Jolla, CA). The sense primer used to remove the *Hind*III site was 5′CTATAGGGAGACCCTCGCTTGGTACCGAGCTC3′. The antisense primer had the respective reverse complementary sequence.

The unique *Hind*III restriction site between the Tat11 and EGFP sequences was used to engineer the following cargo constructs. Tat11-EBFP-EGFP and Tat11-E^{1}GFP-EGFP-tdTomato constructs were obtained by sub-cloning EBFP-EGFP and E^{1}GFP-EGFP-tdTomato in Tat11-EGFP plasmid cut by *Hind*III–*Xba*I to remove the EGFP sequence.

NLS_{SV40}-EGFP plasmid was constructed by two rounds of multiple point mutations onto the sequence of Tat11-EGFP plasmid using the QuickChange Kit (Stratagene). The two primers used in the mutagenesis reactions to transform the Tat11 amino acid sequence in the NLS of SV40 were 5′GGATCCATGTATCCCAAGAAGAAGCGGAAAGTGCGACGA AGA3′ and 5′GAAGCGGAAAGTGGAAGACCCAAAGCTTATAGTGA GC3′. Antisense primers had reverse complementary sequences. NLS_{SV40}-EBFP-EGFP and NLS_{SV40}-E^{1}GFP-EGFP-tdTomato plasmids were constructed by replacing the EGFP sequence of NLS_{SV40}-EGFP plasmid with EBFP-EGFP and E^{1}GFP-EGFP-tdTomato derived from p-EBFP-EGFP and E^{1}GFP-EGFP-tdTomato, respectively (both digested with *Hind*III and *Xba*I restrictions enzymes).

Cell culture and transfections. CHO K1 cells were provided from the American Type Culture Collection (CCL-61 ATCC) and were grown in Ham's F12K medium supplemented with 10% fetal bovine serum at 37 °C and in 5% CO_2. For experiments performed in HeLa (ATCC catalog number CCL-2) cells were growth in Dulbecco's modified Eagle's medium containing 10% (vol/vol) fetal bovine serum and supplemented with glutamine and penicillin/streptomycin.

The transfections of all constructs were carried out using Lipofectamine reagent (Invitrogen, Carlsbad, CA) according to the manufacturer's instructions. For live imaging, 12×10^4 cells were plated 24 hours before transfection onto a 35-mm glass-bottom dish (WillCo-dish GWSt-3522).

For energy depletion studies, cells were incubated for 30 minutes at 37°C in glucose-free Dulbecco's modified Eagle's medium (Invitrogen, Carlsbad, CA) containing 10% fetal bovine serum and supplemented with 10 mmol/l sodium azide and 6 mmol/l 2-deoxy-D-glucose (Sigma, St. Louis, MO). After this treatment, the energy depletion medium was replaced by Dulbecco's modified Eagle's medium, as used in normal growing conditions.

Immunoblotting. Expression of all constructs was confirmed by western blotting. Lysis was performed in a buffer containing 1% Triton X-100, 50 mmol/l HEPES (pH = 7.5), 150 mmol/l NaCl, 10% glycerol, 1.5 mmol/l $MgCl_2$, 5 mmol/l EGTA, 10 μg/ml aprotinin, 10 μg/ml leupeptin. Lysates were then analyzed by sodium dodecyl sulfate polyacrylamide gel electrophoresis and transferred onto nitrocellulose filters. For western blotting procedures, filters were incubated with anti-GFP monoclonal antibody (JL-8, Clontech, Mountain View, CA) and immunodetected with anti-mouse horseradish peroxidase–conjugated secondary antibodies (Amersham Biosciences, Little Chalfont, UK).

Fluorescence microscopy and image analysis. Cell fluorescence was measured using a Leica TCS SP2 inverted confocal microscope (Leica Microsystems AG, Wetzlar, Germany) interfaced with an Ar laser for excitation at 458, 476, 488, and 514 nm, and with an HeNe laser for excitation at 543 and 633 nm. Two-photon excitation of the sample at 760 nm was accomplished by means of an NIR Mira laser (Coherent, CA) with 76-MHz repetition rate and 80-fs laser pulse at source. Glass-bottom Petri dishes containing transfected cells were mounted in a thermostated chamber (Leica Microsystems) and viewed with a 40 × 1.25 numerical aperture oil immersion objective (Leica Microsystems). Live cell imaging was always performed at 37°C. The images were collected using 10–20-μW excitation power at the sample and monitoring the emission by means of the AOBS-based built-in detectors of the confocal microscope. The following collection ranges were adopted: 400–450 nm (Hoechst), 500–550 nm (GFP), 580–650 nm (tdTomato), and 650–750 nm (Mitotracker, Invitrogen, Carlsbad, CA). The background signal has been subtracted from all images. Data were analyzed using the Leica Imaging package, version 2.61, and an implementation of the Igor-Pro software package.

FRAP experiments: nucleus/cytoplasm shuttling. Each FRAP experiment started with a four-time line-averaged image of the cell followed by a single-point bleaching (non-scanning) near the center of the nucleus with a laser pulse at full power (150 μW) for the minimum time required to photobleach most of nuclear fluorescence. Fluorescence of the cytoplasm was photobleached by performing repeated scans of the whole cytoplasmic region with the laser at full power. In each case recovery was measured by starting a time-lapse acquisition within a few milliseconds from the end of bleaching (sampling rate has been tailored to the speed of fluorescence recovery of the tested protein). Each image of the recovery was four-time line-averaged. Image size was 512 × 512 pixels and scan speed was usually set to 400 Hz. The pinhole size was set to the optimal value of 1.0 Airy (corresponding to an 81.44-μm confocal aperture). According to our model of nucleocytoplasmic exchange (**Supplementary Materials and Methods**), collected FRAP curves for both compartments were fitted to mono-exponential equations of the form

$$F_C(t) = F_C^{\infty} + B_C \cdot \exp(-t/\tau), \quad (1)$$

$$F_N(t) = F_N^{\infty} + B_N \cdot \exp(-t/\tau), \quad (2)$$

where $F_C(t)$ and $F_N(t)$ are the fluorescence values at time t of cytoplasm and nucleoplasm, respectively. The three fitting parameters in each equation refer to the asymptotic fluorescence (F_C^{∞}, F_N^{∞}), the dynamic range of recovery (B_C and B_N), and the time constant of exponential decay/recovery (τ). Before fitting, the experimental values of fluorescence were normalized by the fluorescence of the entire cell at the same time, to minimize the effect of cell motility and de-focusing on the recovery curves and to correct for bleaching caused by imaging. Moreover, data were normalized by pre-bleaching fluorescence values to verify the presence of an immobile fraction of fluorescent molecules within the bleached compartment.

FRAP experiments: bleaching of a uniform disk. FRAP measurements were carried out by setting the image format to 64 × 64 pixels, optical zoom to ×32 (resulting pixel width of 183 nm), and pinhole to full open position (7.36 Airy). Scan speed was set to 1,000 Hz in double scanning mode. At least one image was recorded to monitor the fluorescence signal before bleaching. A circle area of 3.5-μm radius within cytoplasm was photobleached using 476-, 488-, and 514-nm light at maximum power (87, 350, and 350 μW, respectively). The photobleaching was completed in approximately 220 milliseconds. Fluorescence recovery was then monitored at 220-millisecond intervals for approximately 8 seconds using 488-nm excitation at 10 μW. Recovery curves have been normalized by a prior time-lapse imaging of the same region without the bleaching step, to verify the presence of an immobile fraction of fluorescent molecules within cytoplasm. Data have been analyzed according to the model proposed by Braeckmans *et al.*,[43] which describes the fluorescence recovery process for a disk-shaped geometry that is photobleached by the scanning beam of a confocal scanning laser microscope. Accordingly, the fluorescence inside the bleached disk (F_{tot}) in the case of a fully opened confocal aperture can be calculated from

$$\frac{F_{tot}}{F_0} = 1 + \left[\sum_{n=1}^{\infty} \frac{(-K_0)^n}{n! \cdot \sqrt{(1+n) + \frac{8Dt}{z_0^2} n}} \right] \cdot \left\{ 1 - \left[I_0\left(\frac{w^2}{2Dt}\right) + I_1\left(\frac{w^2}{2Dt}\right) \right] \cdot \exp\left(-\frac{w^2}{2Dt}\right) \right\}, \quad (3)$$

where F_0 is the total fluorescence inside the disk before bleaching, K_0 is the bleaching parameter (which can be explicitly written in terms of the specific bleaching rate of the fluorophore and zoom setting of the confocal scanning laser microscope),[43] D is the diffusion coefficient, w is the radius of the bleached disk, and z_0 is the axial resolution of the laser point spread function. We experimentally determined the z_0 of our confocal setup (0.7 μm) and fixed the same w value for all FRAP measures (3.5 μm). In contrast, K_0 and D were regarded as fitting parameters.

Determination of transport parameters. The ratio between the protein concentration in the nucleoplasm and cytoplasm (K_{eq}) was determined by taking the ratio between the nuclear (F_N^0) and cytoplasmic fluorescence (F_C^0) before bleaching, *i.e.*, $K_{eq} = F_N^0/F_C^0$. Nuclear volume (V_N) was calculated by assuming an ellipsoid shape for the nucleus with semi-axes d_x, d_y, and d_z, by means of the formula $V_N = (4/3) \cdot \pi \cdot d_x \cdot d_y \cdot d_z$. The three axes were estimated from confocal images of nucleus and in most cases we set d_z equal to d_y, the smallest semi-axis in the horizontal plane. Cytoplasm volume was determined by the relation $B_C \cdot V_C = -B_N \cdot V_N$, which formalizes the mass balance condition between the two compartments (fluorescence is proportional to concentration of unbleached species).

Readers are referred to the **Supplementary Materials and Methods** for **Supplementary Equations [6, 7]** which were used to obtain the diffusive transport parameter (D/W) and the active transport parameter (v^0/C_C^0) from τ, K_{eq}, V_C, and V_N.

ACKNOWLEDGMENTS

We thank Daniele Arosio (Scoula Normale Superiore, NEST CNR–INFM, Pisa) for stimulating and helpful discussions, Laura Marchetti (Scoula Normale Superiore, Pisa) for kindly making available the EBFP-EGFP template,

and Paolo Faraci (Scoula Normale Superiore, NEST CNR–INFM, Pisa) for skilled technical support. We are also grateful to Roger Y. Tsien (University of California, CA) for making available the tdTomato template. This work was partially supported by Fondazione Monte dei Paschi di Siena, Siena, Italy, and the Italian Ministry of University and Scientific Research under FIRB RBLA03ER38.

SUPPLEMENTARY MATERIAL

Figure S1. Schematic representation of the dynamic model proposed in this study.

Materials and Methods.

Figure S2. Cytoplasmic FRAP measurements.

Figure S3. FRAP analysis of Tat1-GFP binding to nucleus.

REFERENCES

1. Raha, T, Cheng, SW and Green, MR (2005). HIV-1 Tat stimulates transcription complex assembly through recruitment of TBP in the absence of TAFs. *PLoS Biol* **3**: e44.
2. Brady, J and Kashanchi, F (2005). Tat gets the "green" light on transcription initiation. *Retrovirology* **2**: 69.
3. Tyagi, M, Rusnati, M, Presta, M and Giacca, M (2001). Internalization of HIV-1 tat requires cell surface heparan sulfate proteoglycans. *J Biol Chem* **276**: 3254–3261.
4. Marcello, A, Cinelli, RA, Ferrari, A, Signorelli, A, Tyagi, M, Pellegrini, V *et al.* (2001). Visualization of *in vivo* direct interaction between HIV-1 TAT and human cyclin T1 in specific subcellular compartments by fluorescence resonance energy transfer. *J Biol Chem* **276**: 39220–39225.
5. Jeang, KT, Xiao, H and Rich, EA (1999). Multifaceted activities of the HIV-1 transactivator of transcription, Tat. *J Biol Chem* **274**: 28837–28840.
6. Brooks, H, Lebleu, B and Vives, E (2005). Tat peptide-mediated cellular delivery: back to basics. *Adv Drug Deliv Rev* **57**: 559–577.
7. Caron, NJ, Torrente, Y, Camirand, G, Bujold, M, Chapdelaine, P, Leriche, K *et al.* (2001). Intracellular delivery of a Tat-eGFP fusion protein into muscle cells. *Mol Ther* **3**: 310–318.
8. Del Gaizo, V and Payne, RM (2003). A novel TAT-mitochondrial signal sequence fusion protein is processed, stays in mitochondria, and crosses the placenta. *Mol Ther* **6**: 720–730.
9. Kalderon, D, Roberts, BL, Richardson, WD and Smith, AE (1984). A short amino acid sequence able to specify nuclear location. *Cell* **39**: 499–509.
10. Robbins, J, Dilworth, SM, Laskey, RA and Dingwall, C (1991). Two interdependent basic domains in nucleoplasmin nuclear targeting sequence: identification of a class of bipartite nuclear targeting sequence. *Cell* **64**: 615–623.
11. Gorlich, D, Kostka, S, Kraft, R, Dingwall, C, Laskey, RA, Hartmann, E *et al.* (1995). Two different subunits of importin cooperate to recognize nuclear localization signals and bind them to the nuclear envelope. *Curr Biol* **5**: 383–392.
12. Gorlich, D, Vogel, F, Mills, AD, Hartmann, E and Laskey, RA (1995). Distinct functions for the two importin subunits in nuclear protein import. *Nature* **377**: 246–248.
13. Smith, A, Brownawell, A and Macara, IG (1998). Nuclear import of Ran is mediated by the transport factor NTF2. *Curr Biol* **8**: 1403–1406.
14. Izaurralde, E, Kutay, U, von Kobbe, C, Mattaj, IW and Gorlich, D (1997). The asymmetric distribution of the constituents of the Ran system is essential for transport into and out of the nucleus. *EMBO J* **16**: 6535–6547.
15. Paine, PL, Moore, LC and Horowitz, SB (1975). Nuclear envelope permeability. *Nature* **254**: 109–114.
16. Truant, R and Cullen, BR (1999). The arginine-rich domains present in human immunodeficiency virus type 1 Tat and Rev function as direct importin beta-dependent nuclear localization signals. *Mol Cell Biol* **19**: 1210–1217.
17. Efthymiadis, A, Briggs, LJ and Jans, DA (1998). The HIV-1 Tat nuclear localization sequence confers novel nuclear import properties. *J Biol Chem* **273**: 1623–1628.
18. Lippincott-Schwartz, J, Snapp, E and Kenworthy, A (2001). Studying protein dynamics in living cells. *Nat Rev Mol Cell Biol* **2**: 444–456.
19. Ormo, M, Cubitt, AB, Kallio, K, Gross, LA, Tsien, RY and Remington, SJ (1996). Crystal structure of the Aequorea victoria green fluorescent protein. *Science* **273**: 1392–1395.
20. Wei, X, Henke, VG, Strubing, C, Brown, EB and Clapham, DE (2003). Real-time imaging of nuclear permeation by EGFP in single intact cells. *Biophys J* **84**: 1317–1327.
21. Farkas, DL, Wei, M, Febbroriello, P, Carson, JH and Loew, LM (1989). Simultaneous imaging of cell and mitochondrial membrane potentials. *Biophys J* **56**: 1053–1069.
22. Calapez, A, Pereira, HM, Calado, A, Braga, J, Rino, J, Carvalho, C *et al.* (2002). The intranuclear mobility of messenger RNA binding proteins is ATP dependent and temperature sensitive. *J Cell Biol* **159**: 795–805.
23. Svoboda, K, Tank, DW and Denk, W (1996). Direct measurement of coupling between dendritic spines and shafts. *Science* **272**: 716–719.
24. Majewska, A, Brown, E, Ross, J and Yuste, R (2000). Mechanisms of calcium decay kinetics in hippocampal spines: role of spine calcium pumps and calcium diffusion through the spine neck in biochemical compartmentalization. *J Neurosci* **20**: 1722–1734.
25. Gerace, L and Burke, B (1988). Functional organization of the nuclear envelope. *Annu Rev Cell Biol* **4**: 335–374.
26. Schindler, M and Jiang, LW (1987). Fluorescence redistribution after photobleaching as a tool for dissecting the control elements of nucleocytoplasmic transport. *Methods Enzymol* **141**: 447–459.
27. Chen, Y, MacDonald, PJ, Skinner, JP, Patterson, GH and Muller, JD (2006). Probing nucleocytoplasmic transport by two-photon activation of PA-GFP. *Microsc Res Tech* **69**: 220–226.
28. Wibo, M and Poole, B (1974). Protein degradation in cultured cells. II. The uptake of chloroquine by rat fibroblasts and the inhibition of cellular protein degradation and cathepsin B1. *J Cell Biol* **63**: 430–440.
29. Lee, DH and Goldberg, AL (1998). Proteasome inhibitors: valuable new tools for cell biologists. *Trends Cell Biol* **8**: 397–403.
30. Moras, D and Poterszman, A (1996). Getting into the major groove. Protein-RNA interactions. *Curr Biol* **6**: 530–532.
31. Siomi, H, Shida, H, Maki, M and Hatanaka, M (1990). Effects of a highly basic region of human immunodeficiency virus Tat protein on nucleolar localization. *J Virol* **64**: 1803–1807.
32. Digman, MA, Sengupta, P, Wiseman, PW, Brown, CM, Horwitz, AR and Gratton, E (2005). Fluctuation correlation spectroscopy with a laser-scanning microscope: exploiting the hidden time structure. *Biophys J* **88**: L33–36.
33. Garcia-Bustos, J, Heitman, J and Hall, MN (1991). Nuclear protein localization. *Biochim Biophys Acta* **1071**: 83–101.
34. Miller, M, Park, MK and Hanover, JA (1991). Nuclear pore complex: structure, function, and regulation. *Physiol Rev* **71**: 909–949.
35. Friedler, A, Friedler, D, Luedtke, NW, Tor, Y, Loyter, A and Gilon, C (2000). Development of a functional backbone cyclic mimetic of the HIV-1 Tat arginine-rich motif. *J Biol Chem* **275**: 23783–23789.
36. D'Agostino, DM, Ciminale, V, Pavlakis, GN and Chieco-Bianchi, L (1995). Intracellular trafficking of the human immunodeficiency virus type 1 Rev protein: involvement of continued rRNA synthesis in nuclear retention. *AIDS Res Hum Retroviruses* **11**: 1063–1071.
37. Henderson, BR and Percipalle, P (1997). Interactions between HIV Rev and nuclear import and export factors: the Rev nuclear localisation signal mediates specific binding to human importin-beta. *J Mol Biol* **274**: 693–707.
38. Fineberg, K, Fineberg, T, Graessmann, A, Luedtke, NW, Tor, Y, Lixin, R *et al.* (2003). Inhibition of nuclear import mediated by the Rev-arginine rich motif by RNA molecules. *Biochemistry* **42**: 2625–2633.
39. Nitin, N, Santangelo, PJ, Kim, G, Nie, S and Bao, G (2004). Peptide-linked molecular beacons for efficient delivery and rapid mRNA detection in living cells. *Nucleic Acids Res* **32**: e58.
40. Neumann, M, Afonina, E, Ceccherini-Silberstein, F, Schlicht, S, Erfle, V, Pavlakis, GN *et al.* (2001). Nucleocytoplasmic transport in human astrocytes: decreased nuclear uptake of the HIV Rev shuttle protein. *J Cell Sci* **114**: 1717–1729.
41. Shaner, NC, Campbell, RE, Steinbach, PA, Giepmans, BN, Palmer, AE and Tsien, RY (2004). Improved monomeric red, orange and yellow fluorescent proteins derived from Discosoma sp. red fluorescent protein. *Nat Biotechnol* **22**: 1567–1572.
42. Ferrari, A, Pellegrini, V, Arcangeli, C, Fittipaldi, A, Giacca, M and Beltram, F (2003). Caveolae-mediated internalization of extracellular HIV-1 tat fusion proteins visualized in real time. *Mol Ther* **8**: 284–294.
43. Braeckmans, K, Peeters, L, Sanders, NN, De Smedt, SC and Demeester, J (2003). Three-dimensional fluorescence recovery after photobleaching with the confocal scanning laser microscope. *Biophys J* **85**: 2240–2252.